Ultrafast Frequency-Shift Dynamics at Temporal Boundary Induced by Structural-Dispersion Switching of Waveguides

Fumiaki Miyamaru, Chihiro Mizuo, Toshihiro Nakanishi, Yosuke Nakata, Kakeru Hasebe, Shintaro Nagase, Yu Matsubara, Yusuke Goto, Joel Pérez-Urquizo, Julien Madéo, and Keshav M. Dani

Phys. Rev. Lett. **127**, 053902 — Published 30 July 2021

DOI: 10.1103/PhysRevLett.127.053902

Ultrafast Frequency-Shift Dynamics at Temporal Boundary Induced by Structural-Dispersion Switching of Waveguides

Fumiaki Miyamaru,[1] Chihiro Mizuo,[1] Toshihiro Nakanishi,[2] Yosuke Nakata,[3] Kakeru Hasebe,[1] Shintaro Nagase,[1] Yu Matsubara,[1] Yusuke Goto,[1] Joel Pérez-Urquizo,[4] Julien Madéo,[4] and Keshav Dani[4]

[1]*Department of Physics, Faculty of Science, Shinshu University, Nagano, Japan.*
[2]*Department of Electronic Science and Engineering, Kyoto University, Kyoto, Japan.*
[3]*Graduate School of Engineering Science, Osaka University, Osaka, Japan.*
[4]*Femtosecond Spectroscopy Unit, Okinawa Institute of Science and Technology Graduate University, Okinawa, Japan.*

(Dated: June 15, 2021)

We experimentally demonstrate the observation of a frequency-shift dynamics at a temporal boundary in the terahertz (THz) region relying on a scheme that controls the structural dispersion of a metal-semiconductor waveguide. Ultrafast structural-dispersion switching is achieved within a sub-picosecond time scale by illuminating a waveguide surface with an optical pump pulse during the propagation of a THz pulse in the waveguide. Owing to the relatively high conversion efficiency, up to 23 %, under the condition that the frequency-shift is sufficiently larger than the bandwidth of the incident pulse, the rapid variation of the THz frequency around the temporal boundary is directly observed in the time domain.

Space-time analogy of spatial phenomena has been fostering exotic physics such as temporal Wood anomaly [1], broadband nonreciprocal application [2], impedance matching beyond Fano-Bode limit [3], and Hawking radiation [4–6]. Among them, a temporal boundary, which is a time-domain counterpart of the spatial boundary between different media is considered as one of the most fundamental elements. It can be established via a sudden change of material parameters of a medium. The frequency of a propagating wave can be abruptly shifted while the incident wavenumber is conserved [7, 8] when it propagates across a temporal boundary, which breaks time-translational symmetry. This frequency shift corresponds to a temporal analog of a change in wavenumber at a spatial boundary that conserves the frequency. In contrast to the frequency conversion based on second or third-harmonic generations with nonlinear materials, the temporal boundary can achieve high frequency conversion efficiency even for weak input signals, in principle [9]. Since such a fascinating frequency shift intrinsically occurs in the time domain, the direct observation of the frequency variation dynamics is essential to pursue exotic physics that occurs at a temporal boundary. To date, frequency conversions with a temporal boundary have been experimentally studied in the microwave to optical frequency ranges with various physical systems, such as rapidly growing plasmas [7, 10–14], photo-excited carriers in semiconductor [15], photonic crystal waveguides [16, 17], and metasurfaces [9, 18, 19]. However, ultrafast dynamics of the frequency shift has not been clearly observed in the time domain because of the difficulty to simultaneously achieve (i) large frequency shifts and (ii) a high conversion efficiency far beyond the noise level of the measured signal.

To satisfy both requirements and directly observe frequency-shift dynamics in the time domain, we propose an effective scheme that aims at temporally modulating the structural-dispersion of a waveguide. Generally, the dispersion relation of a waveguide is determined by its geometric shape and spatial boundary conditions. In our scheme, the structural-dispersion is temporally controlled by generating photo-excited carriers at the surface of metal-semiconductor waveguide structures. The whole pulse propagating in the waveguide can be modulated although only the surface state is switched. Using the proposed scheme, we have derived a theoretical expression of a semi-analytical solution at the temporal boundary, and experimentally demonstrate efficient frequency conversion along with the temporal switching of the structural dispersion of a waveguide in the terahertz (THz) region. The proposed scheme and experimental technique allow us to directly observe the ultrafast dynamics of the electromagnetic wave and accompanying frequency change of the THz wave at the temporal boundary, the time scale of which is much shorter than the period of the THz waves, owing to the generation of photo-excited carriers within a sub-picosecond time scale [20].

First, we introduce basic concepts of structural-dispersion control of waveguides for frequency conversion. We consider that a waveguide is composed of a dielectric slab of relative permittivity ε_r. The slab is located within the $0 \leq y \leq d$ region surrounded by vacuum, and the bottom side at $y = 0$ is metalized with perfect electrical conductor (PEC). For simplicity, we assume that all field distribution is uniform along x. The input electromagnetic wave with frequency $f_{\rm in}$ is a fundamental transverse electric (TE) mode propagating along z in the slab. The dispersion relation between frequency and wavenumber in the z direction of this mode is schematically depicted as a dashed curve in Fig. 1. The circle indicates the location of the frequency and wavenumber of the input electromagnetic wave. When the top side at $y = d$ is suddenly metalized at the time $t = 0$, the propagation mode is converted to eigenmodes as for a double-metalized slab

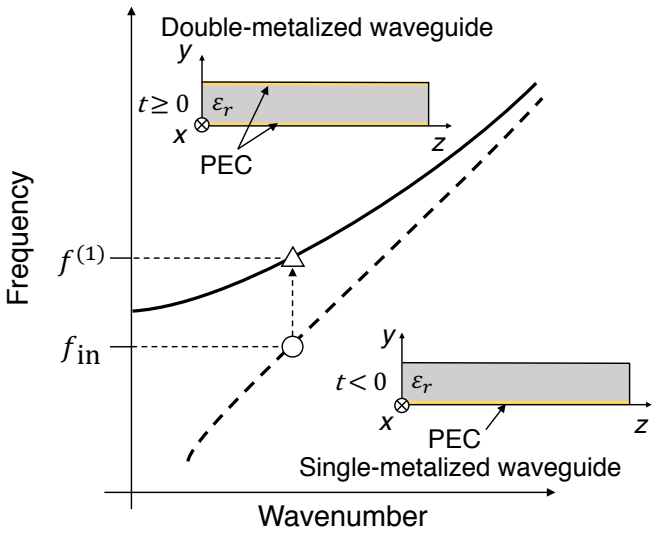

FIG. 1. Schematic diagram of dispersion relations between frequency and wavenumber in z direction for propagation modes in single-metalized (dashed line) and double-metalized (solid lines) waveguides. Insets show the geometric structures of single-metalized (lower one) and double-metalized (upper one) waveguide.

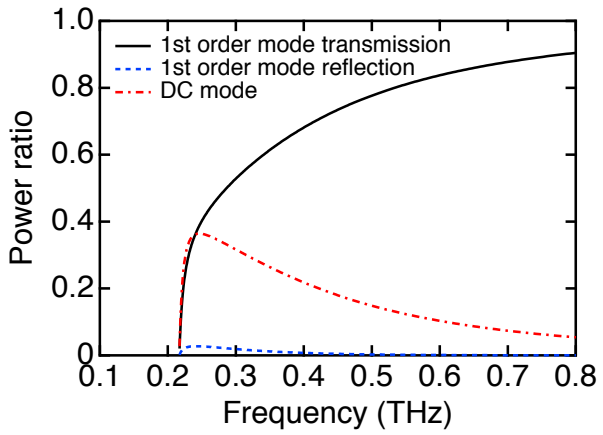

FIG. 2. Theoretically calculated first-order ($l = 1$) power transmission (solid line), reflection (dashed line), and DC conversion ratios (dash-dotted line) as a function of the incident-wave frequency.

(the dispersions as solid curves in Fig. 1). Electric and magnetic fields should be continuous at the time boundary of $t = 0$ [21]; therefore, the wavenumber in z direction must be conserved. Thus, the energy of the incident wave is redistributed to a series of eigenmodes with different frequencies $(f^{(1)}, f^{(2)}, \cdots)$, while the wavenumber is conserved. In Fig. 1, the location of the frequency and wavenumber of the converted electromagnetic wave is indicated as a triangle, and the transition from $f_{\rm in}$ to $f^{(1)}$ is depicted as a dashed arrow. In the above process, we assume that the waveguide is made with a semiconductor and the sudden metallization of the top side is induced by the transient photo-doping in experiments.

Next, we theoretically demonstrate frequency conversion by establishing a rigorous solution for a temporal boundary in a waveguide. To precisely analyze the above situation, we must specify all modes involved in the conversion. We can represent the incident z-component of a magnetic field of angular frequency $\omega_{\rm in}$ and wavenumber in z direction $k_{\rm in}$ for the single-metalized slab as

$$H_z = \begin{cases} A_{\rm in}\cos(k_y y)e^{{\rm j}(\omega_{\rm in}t - k_{\rm in}z)} & (0 \le y \le d) \\ A_{\rm in}\cos(k_y d)e^{-\kappa(y-d)}e^{{\rm j}(\omega_{\rm in}t - k_{\rm in}z)} & (d \le y) \end{cases} \tag{1}$$

with $k_y = \sqrt{\varepsilon_r(\omega_{\rm in}/c_0)^2 - {k_{\rm in}}^2}$ and $\kappa = \sqrt{{k_{\rm in}}^2 - (\omega_{\rm in}/c_0)^2}$, where c_0 is the speed of light in vacuum. All the other field components can be calculated from H_z. By continuously connecting the tangential components of the electric and magnetic fields at the boundary $(y = d)$, we can determine the dispersion relation [22]. For $t \ge 0$, energy is redistributed to modes in the double-metalized slab. Each converted mode inside the waveguide is represented by

$$H_z = A_{\pm}^{(l)}\cos(k_y^{(l)}y)e^{{\rm j}(\pm\omega^{(l)}t - k_{\rm in}z)} \tag{2}$$

where $\omega^{(l)} = 2\pi f^{(l)}$ and $k_y^{(l)}(= l\pi/d)$ are the angular frequency and wavenumber in y direction, respectively. $A_+^{(l)}$ $(A_-^{(l)})$ is the complex amplitude of a wave propagating along $+z$ $(-z)$ with the mode index l, which is corresponding to the transmitted (reflected) electromagnetic wave for the temporal boundary.

However, the modes of Eq. (2) can not represent all the converted fields. This issue is clarified when we consider the magnetic field H_y at the temporal boundary. At $y = d$, the modes expressed by Eq. (2) have no H_y component, while the incident wave has a finite H_y for $t < 0$. Therefore, it is impossible to continuously connect H_y at $(t, y) = (0, d)$. This contradiction can be resolved when we take into account the direct-current (DC) mode in the double-metalized waveguide [22]:

$$H_z = \begin{cases} A_0\cosh(k_{\rm in}y)e^{-{\rm j}k_{\rm in}z} & (0 \le y \le d) \\ -A_0\sinh(k_{\rm in}d)e^{-k_{\rm in}(y-d)}e^{-{\rm j}k_{\rm in}z} & (d \le y). \end{cases} \tag{3}$$

Physically, the DC mode originates from an abrupt change of the conductivity at the top surface of the waveguide. Let us consider the dynamics where $H_y \neq 0$ at $t = -0$ without metal at $y = d$ and the sheet conductivity at $y = d$ is suddenly increased to an infinite value at $t = 0$. At $t = +0$, finite H_y can be trapped, similar to the flux pinning in a superconductor, and hence H_y remains around the top surface as the DC mode.

Considering all modes of Eqs. (1)–(3), we can establish the rigorous solution from the continuous condition

of the electric and magnetic fields at $t = 0$. Thus, the power conversion efficiency can be estimated from the theoretical expression of A_0 and $A_{\pm}^{(l)}$ [22]. Figure 2 shows first-order ($l = 1$) power transmission (solid line), reflection (dashed line), and DC conversion ratios (dash-dotted line) as functions of the incident-wave frequency. Here, we used values of $\varepsilon_r = 12.96$ and $d = 100\,\mu$m. The first-order transmission increases with an increase in the incident frequency. The DC conversion rate shows a peak value at around 0.24 THz. Above 0.24 THz, it decreases with increasing the incident frequency. These dependencies arise because the electromagnetic field distribution in $t < 0$ becomes closer to that of the first-order transmitted mode in $t > 0$ with increasing incident frequency. It should be noted that at lower incident frequencies, the energy transferred to the DC magnetic mode is not negligible.

To directly observe the ultrafast frequency transition that occurs at the temporal boundary in the THz region, we perform an optical-pump THz-probe time domain spectroscopy, which measures the temporal waveform passing through the waveguide. The waveguide utilized in our experiment was made of ∼100-μm-thick semi-insulating gallium arsenide (GaAs), as schematically depicted in Fig. 3(a). The width w and length L of the waveguide were $w \approx 1000$ μm and $L \approx 2500$ μm, respectively. The side surfaces of $d \times w$ were used for input and output of the THz wave. Metal layers of 50-nm platinum, 30-nm titanium and 120-nm gold were deposited on the bottom side of the waveguide. To clearly observe the frequency shift through the conversion process, we restricted the frequency of the incident THz wave to a narrow band using band-pass filters (BPFs). The optical pump pulse of the pulse width ∼100 fs and energy density ∼1.8 μJ/mm^2, illuminates the top surface of $w \times L$ to excite electrons from the valence band to the conduction band of GaAs, producing free carriers in a sub-picosecond time scale. If the plasma frequency of the free carriers is sufficiently high compared to the frequency range of the terahertz wave, the photoexcited GaAs surface can be regarded as a metal. The relative arrival time t_p, which is the timing of the pump-light-pulse irradiation to the waveguide surface relative to the time when the terahertz wave reaches the waveguide, is tuned using the optical delay stage. The THz waves transmitted through the waveguide were detected by an electro-optic sampling technique with a ∼3-mm-thick (110) ZnTe crystal. By varying the relative time of the optical probe pulse to reach the ZnTe crystal with respect to the THz waves, the waveforms of the THz waves were measured. Details of our experimental setup are provided in Supplementary Material [22].

Fig. 3(b) shows waveforms with (solid line) and without (dashed line) optical pumping at the relative pump timing $t_p = 5$ ps. We set t_p as zero when the highest conversion efficiency is obtained. A clear temporal variation of the transmitted THz wave is observed. Both waveforms almost coincide until about 60 ps [22]. An abrupt change of the waveform (solid line in Fig. 3(b)) is observed after 60 ps because of the optical pumping; consequently, we can directly observe the ultrafast frequency-shift in the temporal waveform. Figure 3(c) shows the measured THz waveforms with various optical pump timings. The THz wave transmitted through the waveguide without the optical pumping is also shown, where the frequency remains unconverted. The center frequency of the unconverted THz wave can be seen at 0.48 THz from a Fourier spectrum as shown in Fig. 3(d). With the optical pumping, the converted THz wave can be observed at 0.55 THz. The intensity of the converted peak depends on the optical pump timing. At $t_p = 0$ ps, the converted peak at 0.55 THz reaches a maximum, while the converted peaks are lower for both the earlier ($t_p < 0$) and later ($t_p > 0$) pump timings. This is because at different pump timings the spatial distribution of the incident THz wave coupled in the waveguide is different. Only the incident THz wave existing in the waveguide can contribute to the converted THz wave. For $t_p > 0$, the optical pump pulse reaches the waveguide surface after a part of the THz pulse leaves the waveguide. This brings the unconverted component of the THz wave observed in the time range before 60 ps in Fig. 3(b). On the other hand, for $t_p < 0$, the optical pump pulse reaches the waveguide when only the forward part of the THz pulse enters the waveguide. In this case, the frequency of the backward portion of the THz pulse is not converted. Although this unconverted component is expected to be observed in the delayed time, it was not seen in our experimental result because of the attenuation caused by the Joule loss [22]. The phase of the converted THz wave shifts depending on t_p. This phase shift is attributed to the change of the phase velocity at the temporal boundary. Detailed quantitative analyses are provided in Supplementary Material [22].

To compare input and converted frequencies with the dispersion relation and examine the validity of our experimental results, we measured the frequency conversion characteristics for different carrier frequencies of the incident THz wave using various BPFs. In Fig. 4(a), we show Fourier spectra of the transmitted THz waves without (dashed line) and with (solid line) the optical pumping for several BPFs (BPF-1 – BPF-3). The vertical axis of each figure is normalized by the peak intensity of that without the optical pumping. The BPF-3 is used in Figs. 3(b) and (c). The peak frequencies of the THz wave transmitted through BPF-1, -2, and -3 are 0.35, 0.42, and 0.48 THz, respectively. The optical pump timing is set to obtain the maximum intensity of the converted wave. The converted peak frequencies for BPF-1, -2, and -3 are 0.47, 0.51, and 0.55 THz, respectively. As the frequency variation is much wider than the bandwidth of the incident THz pulse, the frequency

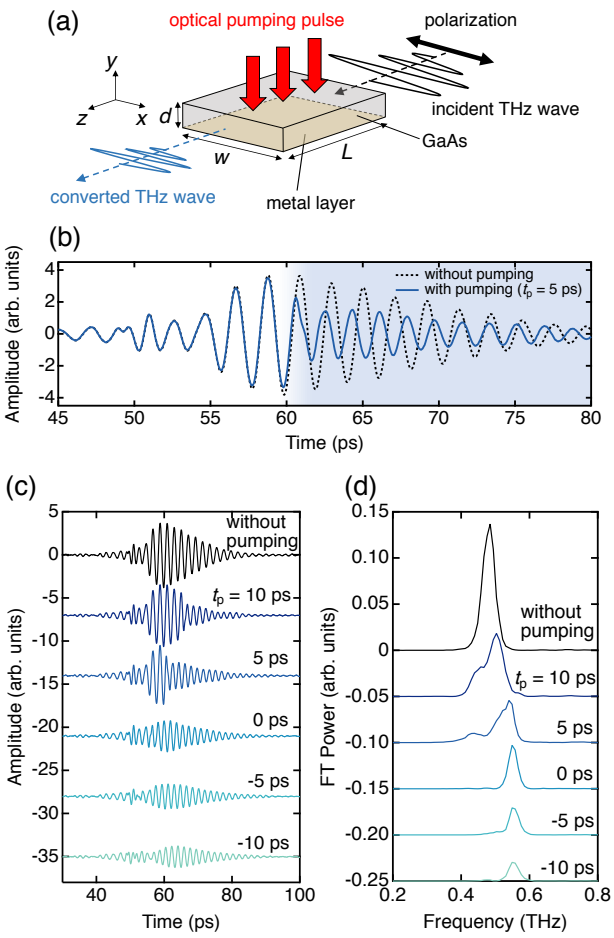

FIG. 3. (a) Schematic picture of a waveguide made of GaAs and optical configuration of incident and outgoing THz waves. The polarization of the incident THz wave is parallel to the metal-deposited surface. (b) Measured waveforms of transmitted THz waves through a waveguide without optical pumping (dashed line) and with optical pumping at $t_p = 5$ ps (solid line). (c) Measured waveforms of transmitted THz waves through a waveguide with various optical pump timings. (d) Corresponding Fourier spectra calculated from (c).

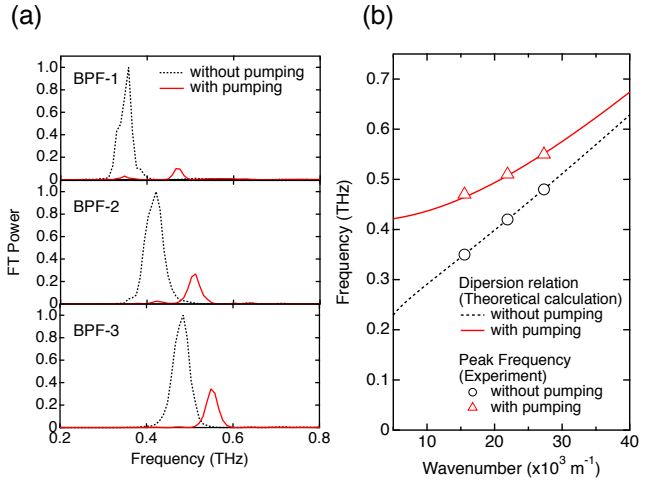

FIG. 4. (a) Fourier spectra without (dashed line) and with (solid line) optical pumping for various BPFs. The vertical axis is normalized by the peak intensity of the spectrum without optical pumping for each figure. (b) Measured peak frequencies (circles and triangles) with theoretically calculated dispersion relations (solid and dashed lines).

upconversions are clearly observed. In Fig. 4(b), we plot experimentally obtained data along with calculated dispersion relations of the fundamental waveguide modes for ε_r =12.96 and d =100 μm [22]. The vertical coordinates of the data (circles and triangles) represent the peak frequencies of the transmitted THz waves without (circle) and with (triangle) the optical pumping. The horizontal coordinate (wavenumber) cannot be directly measured; hence, we deduce it from the theoretical dispersion relation of the single-metalized waveguide with the center frequency of the incident wave. We place triangles at the measured peak frequencies of the output waves with the same wavenumbers, assuming that the wavenumber should be conserved through the temporal boundary. We can confirm that the converted frequencies derived from the experimental results are closely located on the dispersion of the double-metalized waveguide. The agreement certainly justifies the assumption of the wavenumber conservation, which is one of the typical characteristics of the temporal boundary. These experimental results also indicate that the plasma frequency corresponding to photo-excited carriers is sufficiently higher than the frequency region of interest [22].

The conversion efficiency is important if this kind of frequency conversion technique is utilized in practical applications. We estimate the conversion efficiency ($l = 1$) $e = P_w/P_{wo}$, where P_w and P_{wo} are the power obtained by spectrally integrating fitted curves with and without the optical pumping, respectively. The fitting function used in this analysis is a square of a Lorentz function. The conversion efficiencies for BPF-1, -2, and -3 are 8%±1%, 18%±3%, and 23%±2%, respectively. These conversion efficiencies are much higher than those reported in a high-harmonic generation in the THz region [23]. In addition, such high conversion efficiency can be expected, even for a weak THz wave, because it is independent of the input THz power. Compared with the calculated conversion efficiency of the first-order transmission mode shown as a solid line in Fig. 2, there is a possibility to approach the theoretical limit. There are three main possible factors to decrease the conversion efficiency. First, the Ohmic losses of the finite conductivity in coated metal and photo-excited electron-hole pairs could be involved. Second, the finite length of the waveguide could limit the highest conversion efficiency. The incident THz pulses used in our experiment have narrow band spectral widths and correspondingly have tempo-

ral durations of few tens of ps. The waveguide length of 2500 μm is not sufficient to cover the whole component of the incident THz pulse. The THz wave that exists outside the waveguide at the time of the optical pump illumination cannot contribute to the converted THz wave. Third, the coupling coefficient at the output surface of the waveguide is considered. Owing to the change in the propagation mode, the coupling coefficient in the case with optical pumping becomes lower than that without optical pumping, leading to the reduction in measured output power [22]. In principle, some of these limitations can be overcome by using a longer waveguide and a well-designed output coupler.

In conclusion, we have demonstrated the frequency conversion of a THz wave along with the change in the structural-dispersion by illuminating one surface of the waveguide, the other surface of which was coated by metal. The ultrafast change in the THz-pulse frequency is clearly observed in the time domain because thanks to the relatively high conversion efficiency up to 23% and a frequency shift that is sufficiently larger than the bandwidth of the incident wave. Compared to frequency conversion with nonlinear wave mixing in the THz region [23, 24], which generates harmonics at discrete frequencies and requires intense input signal, our method can realize continuous tuning of the output frequency by designing the structure of the waveguide and can achieve a high conversion efficiency even for weak input signals. An unlimited higher frequency shift can be achieved in principle, if the thickness of the double-side metal waveguide is thinner than that of the single-side metal [22]. As an application, our time-domain approach allows to perform frequency conversion for selected pulses in a pulse train [22]. As for further advanced conversion, a pump beam with spatially modulated intensity [25, 26], which is used for improving the efficiency of high-order harmonic generation, is available. In our scheme, there is a possibility of effectively and selectively converting to the higher-order propagation modes by using spatially patterned beams. We believe that this structural-dispersion approach for realizing the temporal boundary will be useful for future applications in THz waves.

This study was partially supported by JSPS KAKENHI Grant Number JP19K05304, Inamori Foundation, and JST, PRESTO Grant Number JPMJPR20L6. The authors acknowledge Dr. Katsuya Teshima's group at Shinshu University and Dr. Alexander Badrutdinov at Okinawa Institute of Science and Technology Graduate University for their experimental supports. F. M. also acknowledges Mr. Yuichi Honma, Dr. Keisuke Takano, and Dr. Masahiko Higuchi at Shinshu University for fruitful discussions.

[1] E. Galiffi, Y.-T. Wang, Z. Lim, J. B. Pendry, A. Alú, and P. A. Huidobro, Phys. Rev. Lett. **125**, 127403 (2020).
[2] E. Galiffi, A. A. Huidobro, and J. B. Pendry, Phys. Rev. Lett. **123**, 206101 (2019).
[3] A. Shlivinski and Y. Hadad, Phys. Rev. Lett. **121**, 204301 (2018).
[4] S. Weinfurtner, E. W. Tedford, M. C. J. Penrice, W. G. Unruh, and G. A. Lawrence, Phys. Rev. Lett. **106**, 021302 (2011).
[5] R. J. Doornenbal, A. Roldán-Molina, A. S. Nunez, and R. A. Duine, Phys. Rev. Lett. **122**, 037203 (2019).
[6] J. Drori, Y. Rosenberg, D. Bermudez, Y. Silberberg, and U. Leonhardt, Phys. Rev. Lett. **122**, 010404 (2019).
[7] S. C. Wilks, J. M. Dawson, and W. B. Mori, Phys. Rev. Lett. **61**, 337 (1988).
[8] Y. Xiao, G. P. Agrawal, and D. N. Maywar, Opt. Lett. **36**, 505 (2011).
[9] K. Lee, H. Son, J. Park, B. Kang, W. Jeon, F. Rotermund, and B. Min, Nat. Photonics **12**, 765 (2018).
[10] S. P. Kuo, Phys. Rev. Lett. **65**, 1000 (1990).
[11] S. P. Kuo, A. Ren, and G. Schmidt, Phys. Rev. E **49**, 3310 (1994).
[12] N. Yugami, T. Niiyama, T. Higashiguchi, H. Gao, S. Sasaki, H. Ito, and Y. Nishida, Phys. Rev. E **65**, 036505 (2002).
[13] J. Faith, S. P. Kuo, and J. Huang, Phys. Rev. E **55**, 1843 (1997).
[14] S. P. Kuo and J. Faith, Phys. Rev. E **56**, 2143 (1997).
[15] A. Nishida, N. Yugami, T. Higashiguchi, T. Otsuka, F. Suzuki, M. Nakata, Y. Sentoku, and R. Kodama, Appl. Phys. Lett. **101**, 161118 (2012).
[16] J. Upham, Y. Tanaka, T. Asano, and S. Noda, Appl. Phys. Express **3**, 062001 (2010).
[17] T. Kampfrath, D. M. Beggs, T. P. White, A. Melloni, T. F. Krauss, and L. Kuipers, Phys. Rev. A **81**, 043837 (2010).
[18] K. Lee, J. Park, J. Son, B. J. Kang, W. T. Kim, S. C. Lee, B. Min, and F. Rotermund, Opt. Express **27**, 12762 (2019).
[19] A. M. Shaltout, V. M. Shalaev, and M. L. Brongersma, Science **364**, 648 (2019).
[20] R. Huber, F. Tauser, A. Brodschelm, M. Bichler, G. Abstreiter, and A. Leitenstorfer, Nature **414**, 286 (2001).
[21] K. Qu, Q. Jia, M. R. Edwards, and N. J. Fisch, Phys. Rev. E **98**, 023202 (2018).
[22] See Supplementary Material at (URL) for detailed discussion on theoretical model, experimental setup, temporal position of temporal boundary, transmission characteristic for broadband pulse, phase-velocity change, pump-power dependence, analysis of coupling coefficient, spectral tunability in frequency conversion, and selected conversion for multipulses.
[23] H. A. Hafez, S. Kovalev, J.-C. Deinert, Z. Mics, B. Green, N. Awari, M. Chen, S. Germanskiy, U. Lehnert, J. Teichert, Z. Wang, K.-J. Tielrooij, Z. Liu, Z. Chen, A. Narita, K. Mullen, M. Bonn, M. Gensch, and D. Turchinovich, Nature **561**, 507 (2018).
[24] P. Bowlan, E. Maritnez-Moreno, K. Reimann, T. Elsaesser, and M. Woerner, Phys. Rev. B **89**, 041408(R) (2014).
[25] C. Altucci, R. Bruzzese, D. D'Antuoni, C. de Lisio, and

S. Solimeno, J. Opt. Soc. Am. B **17**, 34 (2000).
[26] J. J. J. Nivas, E. Allahyari, F. Cardano, A. Rubano, R. Fittipaldi, A. Vecchione, D. Paparo, L. Marrucci, R. Bruzzese, S. Amoruso, Appl. Sur. Sci. **471**, 1028 (2019).